Chemical and biological sensors

Multiwell Plate Impedance Analysis of a Nanowell Array Sensor for Label-Free Detection of Cytokines in Mouse Serum

Seyed Reza Mahmoodi[1], Pengfei Xie[1], Mark Allen[2,*], and Mehdi Javanmard[1,**]

[1]S. R. Mahmoodi, P. Xie, and M. Javanmard are with the Department of Electrical and Computer Engineering, Rutgers University, Piscataway, NJ 08854 USA

[2]M. Allen is with the Department of Electrical and Systems Engineering, University of Pennsylvania, Philadelphia, PA 19104 USA

*Fellow, IEEE

**Member, IEEE

Manuscript received November 5, 2019; revised December 31, 2019; accepted January 15, 2020. Date of publication January 22, 2020; date of current version February 10, 2020.

Abstract— We present a novel method for label-free detection of tumor necrosis factor alpha (TNF-α) in serum after immobilization by electric field. Detection of proteins in blood using label-free impedance-based techniques is difficult due to high salt concentration of the matrix, which results in charge screening. The nanowell array sensor provides enhanced electrochemical sensitivity by electric field focusing in the nanoscale volume wells. Here, an on-chip multiwell plate sensing platform was fabricated and tested. The sensor performance through testing in mouse serum at protein concentrations between 10 and 500 ng/l has been demonstrated. This detection modality is advantageous to many label-free electronic sensors in that signal power scales will increase in salt concentration, thus improving the sensitivity of the platform.

Index Terms—Chemical and biological sensors, biosensors, electrochemical impedance spectroscopy (EIS), label free, nanowell, protein.

I. INTRODUCTION

Measurement of various specific proteins in body fluids can be a key component of continuous health monitoring. The common techniques for protein quantification usually rely on labeling and optical fluorescence [1]. As an alternative approach, electrochemical impedance analyses have been recognized as a powerful tool for different types of sensor applications due to significant advantages, such as inherent simplicity, rapid response, high sensitivity, and low cost [2].

In the field of biosensors, electrochemical impedance spectroscopy (EIS) based sensors are known as promising candidates since they benefit from ease of miniaturization, reliability in detecting biomarkers, and label-free operation. These sensors are particularly well-suited to detect binding events on the transducer surface, which makes them ideal candidates for detection of deoxyribonucleic acid (DNA) and proteins [3]. One drawback of these sorts of microsystems is that direct immobilization of antibodies on the electrode surface impedes the repeated use of impedance biosensors and causes problems in their calibration due to random antibody orientation and subsequent decreased availability of antibody active sites [4]. Therefore, strategies such as particle-based impedance sensing have been proposed that involve magnetic beads or gold nanoparticle labeling to reuse the sensor [5]. However, sensitivity in these systems is usually low, and the labeling process detracts from the primary goal of label-free detection.

Multiwell plate assays present suitable conditions for screening biological or chemical libraries in static fluid environments in which many samples can be analyzed in parallel [6]. These platforms can be combined with impedance-based biosensors to improve both the sensitivity and efficiency, since it promotes attachment of antibody to the electrode surface and enables simultaneous detection of different analytes by immobilizing their respective ligands on separate electrodes [7]. Moreover, these assays can provide real-time analysis of cells in culture without the need for enzymatic stripping, fluorescent dyes, fixatives, or other perturbations [8].

Here, the nanowell array electrodes were designed as a platform to carry out the dual functions of electric field antibody immobilization and providing a highly sensitive EIS platform. The electric field focusing [5], [9] was employed to immobilize probe antibody more uniformly to minimize the unwanted nonspecific binding or aggregation of antibody molecules inside the nanowells [4]. In this article, a wafer-scale sensing configuration with 40-nm-electrode gap has been described. The presented nanowell array functionalized biosensor demonstrates a dynamic range of 10–500 ng/l for tumor necrosis factor alpha (TNF-α) in mouse serum with a limit of detection of 10 ng/l. Robust performance through repeated testing in mouse serum was determined by extracting a calibration curve.

II. NANOWELL ARRAY SENSOR

The nanowell array biosensors have significantly improved label-free detection by providing highly sensitive analyses [10], [11]. In the current study, the designed sensor is comprised of a 20×20 μm^2 overlap area at the tip of the two confronting electrodes with 25 individual nanowells. The sensor was fabricated by patterning gold electrodes on a glass substrate. Connection pads are fabricated on opposing sides of the chip with traces leading to the center of the chip. The two electrodes overlap with each other and are separated by a thin aluminum oxide layer. The micropatterned holes expose the bottom electrode to the test solution and the probe antibody of tumor necrosis factor alpha (anti-TNF-α) can be immobilized inside the nanowells by the electric field focusing.

Fig. 1 shows the assembled device and a schematic of the nanowell, comprising a pair of gold electrodes, separated by a 40-nm insulator layer. The entire chip consists of 28 sensors in separate polydimethylsiloxane (PDMS) wells. Binding of target antigen will modulate the impedance between the electrodes, resulting in a change in the

Corresponding author: Seyed Reza Mahmoodi (reza.mahmoodi@rutgers.edu).
Associate Editor: I. Papautsky.
Digital Object Identifier 10.1109/LSENS.2020.2968214

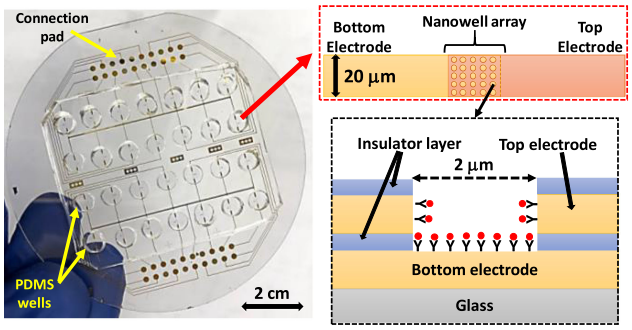

Fig. 1. Entire multiwell plate chip and a schematic view of the 2-μm array sensor. The sensor is comprised of an array of 25 nanowells etched on the overlapping electrode surface.

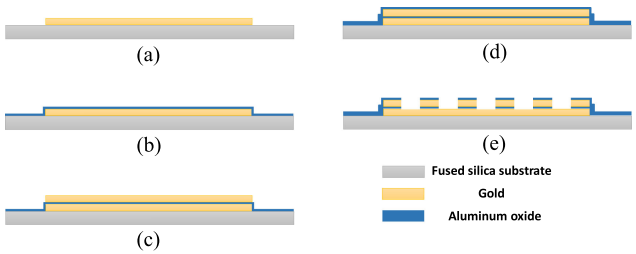

Fig. 2. Fabrication steps of the naowell array sensor. Cross-sectional views of the micropatterned wells on the overlapping region. (a) Patterning the bottom gold electrode, (b) ALD of interelectrode aluminum oxide layer, (c) patterning the top gold electrodes, (d) ALD of second layer of aluminum oxide, and (e) ion milling step to create the nanowell array.

impedance spectra due to partial occlusion of charges passing between the two electrodes. Higher salt concentration results in larger current, thus higher signal power corresponding to larger changes in current due to protein binding, making the sensor ideal for quantification of proteins in high salt content matrices, such as serum [12].

In the nanowell array sensor, most of the gold electrode area is covered with an aluminum oxide layer such that only a limited surface of the electrodes is exposed to the test solution inside the nanowells. Therefore, this geometry would limit the amount of probe antibody molecules inside the nanowell and thus can provide more sensitive detection of surface binding events. Furthermore, the small surface of the electrodes can improve the sensitivity by concentrating the electric field into a small volume inside the nanowells. Moreover, electric field immobilization can align antibody molecules along the electric field to enhance the sensor performance [13].

III. MATERIALS AND METHODS

The processing steps of the sensor structure are demonstrated in Fig. 2. First, a bare fused silica wafer (University Wafer, South Boston, MA, USA) was cleaned by oxygen plasma. Then, a layer of 150-nm-thick gold was deposited on the wafer by e-beam evaporation and patterned by lift-off, yielding the bottom layer electrode. Atomic layer deposition (ALD) was used to deposit a 40-nm-aluminum-oxide film as an interelectrode insulator. The top gold electrode, the interconnecting lines, and the connection pads (150 nm) were patterned using the same method as for the bottom layer electrode. Five-nm layers of chromium and aluminum were coated by e-beam and thermal evaporation, respectively, to enhance the adhesion of the gold electrodes and the aluminum oxide layer to their corresponding substrates. Next, another 40-nm passivation layer of aluminum oxide was deposited on top of this structure by ALD. Finally, the nanowells were patterned in the overlapping part of the two electrodes and etched by ion milling to fabricate the nanowell array. Gold connection pads of the bottom electrodes were protected by small pieces of Kapton tape during the entire fabrication procedure. Thereafter, a PDMS block with 28 holes was bonded to the wafer by oxygen plasma treatment to fluidically isolate each sensor pairs and to create the multiwell plate design (see Fig. 1).

EIS experiments on the sensors were performed using a potentiostat (Gamry Reference 600, Gamry Instruments, Warminster, PA, USA) in a two-electrode configuration. Before EIS testing, the wells were washed with ethanol, deionized water and phosphate buffered saline (PBS) to remove any contamination or dielectric material from the sensor surface. A lock-in-amplifier (HF2IS-MF multifrequency, Zurich Instruments, Zurich, Switzerland) is used to apply voltage and monitor the impedance across the electrodes continuously in realtime. In each set of experiments, the EIS measurements were first conducted in 20 μL of PBS, and then, by EIS measurement and real-time impedance monitoring, it was ensured that small additions of PBS do not impact the impedance after reaching a plateau. After stabilization of the impedance signal, anti-TNF-α (40 μM in 1$\times$ PBS; MW$\sim$150 kDa; R&D Systems, Minneapolis, MN, USA) was added into the PDMS well and immobilized by applying 100 mV at 100 kHz for about 20 min. Addition of the same volume of PBS was recorded on a separate sensor to compare the real-time response of the sensor.

After functionalizing by anti-TNF-α, the EIS spectra were recorded to ensure the antibody attachment on the electrode surface inside the nanowells. 2 μL of blank PBS and nonspiked serum (Sigma Aldrich, St. Louis, MO, USA) was inserted into different fluidic cells as negative control. The purpose of this step is to remove the possible effects from PBS and serum in the sensor measurements because anti-TNF-α and TNF-α were diluted in 1$\times$ PBS. Finally, the target cytokine, TNF-α (MW$\sim$17.3 kDa; R&D Systems, Minneapolis, MN, USA), was suspended in concentrations ranging from 10 to 500 ng/l. The target cytokine buffer at a concentration of 0.2 mg/ml (in 1$\times$ PBS) was mixed with pure mouse serum before each experiment. For each step, complete stabilization and recording of the spectra across the electrodes took less than 30 min.

At each stage of fluid addition, impedance measurements were conducted in 10-mV amplitude between working and counter electrodes using a frequency range 100–1 000 000 Hz to produce EIS curves. Sensors were isolated from external electromagnetic interference using a Faraday cage, significantly reducing external interference and allowing for reliable measurements. EIS parameters were generated by fitting the data to the Randles' equivalent circuit model using Gamry Electrochem software. Every addition test was conducted three times to obtain averaged results. The obtained impedance data were converted to capacitance values using $C = -1/\omega Z''$, where C is the capacitance, ω is the angular frequency, and Z'' is the imaginary part of the impedance.

IV. RESULTS AND DISCUSSION

Fig. 3 shows low and high magnification images of the sensor electrodes, confirming the successful formation of nanowells on the overlapping electrode surface by the ion milling process. An array of 2-μm-well is embedded into the overlapping area to create a conductive path between the top and bottom electrodes via the test solution. The chip contains 28 sensors that can be used to do highly selective multiplexed detection of protein in parallel experiments.

Here, EIS measurements were performed to detect target cytokine in mouse serum at low concentrations. These spectra in the form of

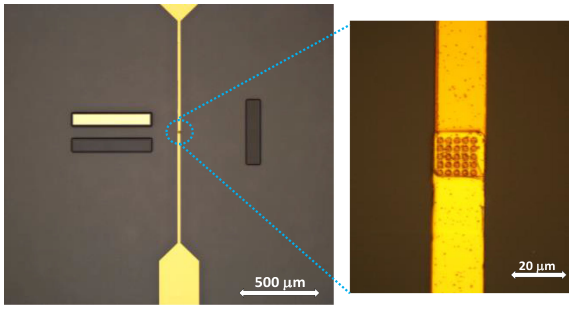

Fig. 3. Microscopic images of fabricated sensors at low and high magnifications, showing the produced array of nanowells at the tip of the two confronting electrodes.

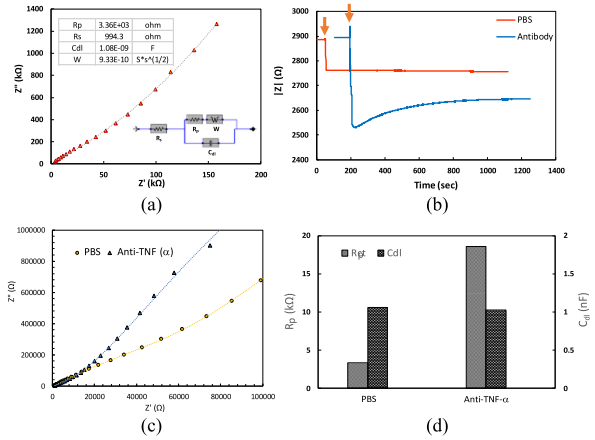

Fig. 4. (a) EIS testing in 1× PBS. The inset shows the fitted equivalent circuit Randles model, and the resulting values based on the fitted data. (b) Real-time monitoring of stabilization time with a lock-in-amplifier at 100 kHz, (c) Nyquist plots, and (d) polarization resistance (R_p) and double layer capacitance (C_{dl}) of the sensor before and after anti-TNF-α attachment.

Nyquist plots can be fitted to a Randles' equivalent for interpretation. EIS test was initially performed in the purified buffer. The EIS data after 20 μL of 1× PBS was introduced onto the washed electrodes are shown in Fig. 4(a). By fitting the experimental data into the Randles′ model, the components of the model can be derived as presented in the inset. The listed parameters include solution resistance (R_s), polarization resistance (R_p), double-layer capacitance (C_{dl}), and Warburg element for diffusion (W). In Fig. 4(a), the high-frequency region shows a small incomplete semicircle, whereas the medium- and low-frequency ranges of the graph show a Warburg-type impedance behavior, which can be related to the diffusion of ions within the solution [14].

Prior to any insertion tests, nanowells were functionalized with antibody by applying a voltage across the electrodes. The real-time impedance measurement of anti-TNF-α immobilization is illustrated in Fig. 4(b). On a different device, real-time impedance monitoring was also performed with blank PBS addition to be compared with anti-TNF-α curve. In both conditions, the impedances across the electrodes decrease immediately due to the increased conductivity of the solution, which are marked with arrows. However, physical immobilization of the antibody inside the nanowells increases the baseline over a time period of several minutes and reaches a plateau by 15 min. The EIS plots of the sensor recorded before and after antibody functionalization are shown in Fig. 4(c), and the derived values for R_p and C_{dl} are illustrated in Fig. 4(d). The increase in R_p is consistent with

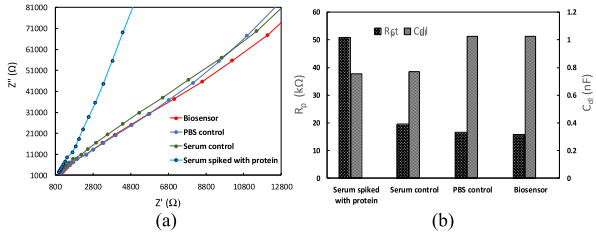

Fig. 5. (a) Nyquist plots and (b) polarization resistance R_p and double layer capacitance C_{dl} measured in three separate experiments; target protein concentration is 500 ng/l.

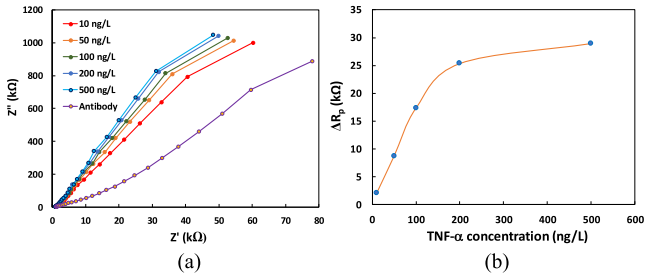

Fig. 6. (a) EIS response to the sample spiked with target protein at different concentrations. EIS measurement of the functionalized biosensor is also included. (b) Calibration plot showing the change of polarization resistance as a function of the different concentrations of target protein.

the presence of antibody in the nanowells, which reduces its surface conductivity. The obtained results from circuit fitting also showed that the immobilization of antibodies in the nanowells did not effectively change the double layer capacitance, nor the Warburg impedance, similar to observations in [15] and [16].

After functionalization of the patterned electrode, we evaluated the ability of the biosensor to detect TNF-α protein in mouse serum. Therefore, three identical biosensors were exposed to additions of blank PBS and spiked and nonspiked mouse serum in parallel measurements. For negative control experiments, we used both PBS and nonspiked serum, since the target protein was diluted in PBS. The EIS response of the biosensor to different fluid additions are presented as Nyquist plots in Fig. 5(a). Also, the results for the generated R_p and C_{dl} are shown in Fig. 5(b), where R_p is the parameter used to evaluate analyte biosensor binding in the experiments, which indicate a difference in the dielectric or conductive properties of the electrode surface [17], [18]. For the negative control test, when serum containing no protein was added into the fluidic cell, aside from the small decrease in the double layer capacitance, polarization resistance did not increase noticeably. This demonstrates the capability of the nanowell array sensor to detect serum spiked with 500 ng/l of TNF-α. Also, the slight decrease in the capacitance by serum addition can be associated with the changes in the total ionic concentration of the solution.

In Fig. 5, similar to antibody immobilization, the most significant change was found in the polarization resistances. For the negative control step, when blank PBS was added into the fluidic cell, almost no change in R_p and C_{dl} was observed. As shown in Fig. 5(b), although serum addition to PBS medium slightly decreases the solution resistance, probably due to high salt concentration of complex biological species, the serum control addition also does not significantly change R_p.

A titration experiment was performed to determine sensor response as a function of analyte concentration in serum. The Nyquist plots of

impedance spectra with various concentrations of TNF-α in serum are shown in Fig. 6(a). Fig. 6(b) shows the calibration plot that corresponds to the values of R_p differences (ΔR_p) of the biosensor before and after the spiked serum addition. As seen in Fig. 6(b), the sensor shows a linear trend at concentrations lower than 200 ng/l. Considering the blank and the signal fluctuation, the detection limit for the binding of TNF-α on the system is found to be 10 ng/l.

V. CONCLUSION

In this article, we presented a nanowell array impedance sensor for label-free detection of cytokines and other biomarkers. The electrode structure is composed of two opposing electrodes such that the overlapping region of the two electrodes is separated by a thin oxide layer and micropatterned with holes that expose the bottom electrode to solution. By monitoring the impedance across the electrodes after sensor functionalization with antibody, we recorded the EIS measurements at each stage of the fluid additions. Fitting the data to Randles' equivalent circuit model demonstrated that reliable detection of TNF-α is possible at a dynamic range between 10 and 500 ng/l. Negative control measurements were performed using blank mouse serum and PBS to ensure that sensor fouling did not result in false positive signals.

ACKNOWLEDGMENT

This work was supported by DARPA Cooperative Agreement HR0011-16-2-0026 under the ElectRX program managed by Dr. E. V. Giesen.

REFERENCES

[1] A. M. Coto-García, E. Sotelo-González, M. T. Fernández-Argüelles, R. Pereiro, J. M. Costa-Fernández, and A. Sanz-Medel, "Nanoparticles as fluorescent labels for optical imaging and sensing in genomics and proteomics," *Anal. Bioanal. Chem.*, vol. 399, no. 1, pp. 29–42, 2011.

[2] C. Zhu, G. Yang, H. Li, D. Du, and Y. Lin, "Electrochemical sensors and biosensors based on nanomaterials and nanostructures," *Anal. Chem.*, vol. 87, pp. 230–249, 2015.

[3] A. Merkoçi, "Nanoparticles-based strategies for DNA, protein and cell sensors," *Biosensors Bioelectron.*, vol. 26, no. 4. pp. 1164–1177, 2010.

[4] A. Makaraviciute and A. Ramanaviciene, "Site-directed antibody immobilization techniques for immunosensors," *Biosensors Bioelectron.*, vol. 50, pp. 460–471, 2013.

[5] K. S. Shin, J. H. Ji, K. S. Hwang, S. C. Jun, and J. Y. Kang, "Sensitivity enhancement of bead-based electrochemical impedance spectroscopy (BEIS) biosensor by electric field-focusing in microwells," *Biosensors Bioelectron.*, vol. 85, pp. 16–24, 2016.

[6] J. Y. Kim, D. A. Fluri, J. M. Kelm, A. Hierlemann, and O. Frey, "96-well format-based microfluidic platform for parallel interconnection of multiple multicellular spheroids," *J. Lab. Autom.*, vol. 20, no. 3, pp. 274–282, 2015.

[7] J. Paredes, S. Becerro, F. Arizti, A. Aguinaga, J. L. Del Pozo, and S. Arana, "Interdigitated microelectrode biosensor for bacterial biofilm growth monitoring by impedance spectroscopy technique in 96-well microtiter plates," *Sensors Actuators B, Chem.*, vol. 178, pp. 663–670, 2013.

[8] H. Li, J. Somerson, F. Xia, and K. Plaxco, "Electrochemical DNA-based sensors for molecular quality control: continuous, real-time melamine detection in flowing whole milk," *Anal. Chem.*, vol. 90, no. 18, pp. 10641–10645, 2018.

[9] S. Emaminejad, M. Javanmard, C. Gupta, S. Chang, R.W. Davis, and R. T. Howe, "Tunable control of antibody immobilization using electric field," *Proc. Nat. Acad. Sci. USA*, vol. 112, no. 7, pp. 1995–1999, 2015.

[10] Z. Namhil *et al.*, "A label-free aptamer-based nanogap capacitive biosensor with greatly diminished electrode polarization effects," *Phys. Chem. Chem. Phys.*, vol. 21, no. 2, pp. 681–691, 2019.

[11] Y. Seo, S. Jeong, J. Lee, H. S. Choi, J. Kim, and H. Lee, "Innovations in biomedical nanoengineering: Nanowell array biosensor," *Nano Convergence*, vol. 5, no. 1, 2018, Art. no. 9.

[12] N. Song, P. Xie, W. Shen, M. Javanmard and M. G. Allen, "Microwell-array on a flexible needle: A transcutaneous insertable impedance sensor for label-free cytokine detection," in *Proc. IEEE Micro Electro Mech. Syst.*,2018, pp. 392–395.

[13] E. Matysiak-Brynda, B. Wagner, M. Bystrzejewski, I. P. Grudzinski, and A. M. Nowicka, "The importance of antibody orientation in the electrochemical detection of ferritin," *Biosensors Bioelectron.*, vol. 109, pp. 83–89, 2018.

[14] J. Macdonald and E. Barsoukov, *Impedance Spectroscopy: Theory, Experiment, and Applications*, vol. 113. Hoboken, NJ, USA: Wiley, 2005, pp. 13103–13107.

[15] X. Wang *et al.*, "Three-dimensional graphene biointerface with extremely high sensitivity to single cancer cell monitoring," *Biosensors Bioelectron.*, vol. 105, pp. 22–28, 2018.

[16] J. Rushworth, A. Ahmed, H. Griffiths, N. Pollock, N. Hooper, and P. Millner, "A label-free electrical impedimetric biosensor for the specific detection of Alzheimer's amyloid-beta oligomers," *Biosensors Bioelectron.*, vol. 56, pp. 83–90, 2014.

[17] Y. Hou *et al.*, "Immobilization of rhodopsin on a self-assembled multilayer and its specific detection by electrochemical impedance spectroscopy," *Biosensors Bioelectron.*, vol. 21, no. 7, pp. 1393–1402, 2006.

[18] F. Darain, D. S. Park, J. S. Park, and Y. B. Shim, "Development of an immunosensor for the detection of vitellogenin using impedance spectroscopy," *Biosensors Bioelectron.*, vol. 19, no. 10, pp. 1245–1252, 2004.